Nanocontact resistance and structural disorder induced resistivity variation in metallic metal-oxide nanowires

2009 Nanotechnology 20 455401

(http://iopscience.iop.org/0957-4484/20/45/455401)

Nanotechnology **20** (2009) 455401 (7pp) doi:10.1088/0957-4484/20/45/455401

Nanocontact resistance and structural disorder induced resistivity variation in metallic metal-oxide nanowires

Y F Lin[1], Z Y Wu[2], K C Lin[2], C C Chen[2], W B Jian[1], F R Chen[2] and J J Kai[2]

[1] Department of Electrophysics, National Chiao Tung University, Hsinchu 30010, Taiwan
[2] Department of Engineering and System Science, National Tsing Hua University, Hsinchu 30013, Taiwan

E-mail: wbjian@mail.nctu.edu.tw

Received 28 May 2009, in final form 14 September 2009
Published 13 October 2009
Online at stacks.iop.org/Nano/20/455401

Abstract

Several systems of metallic metal-oxide nanowires (NWs), including pure RuO_2 and as-implanted and annealed $Ru_{0.98}Cu_{0.02}O_2$ and $Ru_{0.93}Cu_{0.07}O_2$ NWs, have been employed in two-probe electrical characterizations by using a transmission electron microscope–scanning tunneling microscope technique with a gold tip. Thermal, mechanical, and electron beam exposing treatments are consecutively applied to reduce the electrical contact resistance, generated from the interface between the NW and the gold tip, so as to evaluate the intrinsic NW resistance. It is found that the residual contact resistance cannot be entirely removed. For each system of metallic metal-oxide NWs, several tens of NWs are applied to electrical characterizations and the total resistances unveil a linear dependence on the ratio of the length to the area of the NWs. As a result, the average resistivity and the contact resistance of the metallic metal-oxide NWs could be evaluated at room temperatures. The average resistivities of pure RuO_2 NWs agree well with the results obtained from standard two- and four-probe electrical-transport measurements. In addition, the as-implanted Cu–RuO_2 NWs reveal disordered crystalline structures in high-resolution TEM images and give higher resistivities in comparison with that of pure RuO_2 NWs. The residual contact resistances of all kinds of metallic metal-oxide NWs unveil, more surprisingly, an approximation value of several kilohms, even though the average resistivities of these NWs change by more than one order of magnitude. It is argued that the ductile gold tip makes one or more soft contacts on the stiff metal-oxide NWs with nanometer roughness and the nanocontacts on the NWs contribute to the electrical contact resistance.

(Some figures in this article are in colour only in the electronic version)

1. Introduction

Theoretical studies on the electrical contact resistance (ECR) of rough surfaces, modeled as a number of clusters of microcontact spots, are of essential significance due to their fruitful applications in electromechanical switches, relays, wire bonding, and tribology [1, 2]. As the constriction of electrical contact is reduced to a single microcontact spot with a cross-sectional diameter larger than the electrons' mean free path, it manifests itself in ECR as a Maxwell resistance of $\rho/2r$ [3], where ρ and r are the resistivity and cross-sectional radius, respectively. On the other hand, if the cross-sectional diameter of a microcontact is smaller than the electrons' mean free path, the ECR reveals a conducting channel with a quantized resistance of $h/2e^2$ ($\sim$13 kΩ), where h and e are the Plank's constant and electron charge, respectively. In particular, not only the semiclassical Sharvin approximation but also the scattering approach of the Landauer formula give the same fundamental resistance unit [3, 4]. Quantization of the ballistic resistance has been experimentally demonstrated

in a two-dimensional electron gas of a semiconductor heterojunction [5, 6]. In addition, experimental verification on the quantized ECR through a three-dimensional metal point contact were established using a mechanical break junction [7], scanning tunneling microscope [8, 9], electromechanical relays [10], solid electrochemical reaction [11], and other novel gadgets [12, 13]. It was argued that both electronic and mechanical properties, such as an atomic d orbital and different arrangements of atomic chains will modulate the quantized ECR [14].

Metallic metal-oxide materials such as RuO_2 are inviting electrical contact materials [15], and furthermore, they are transparent to light so are potential candidates to be employed in display technology. Actually, electrical characterizations for the ECR of the metallic metal-oxide nanowires (NWs) are essential due to possible applications to interconnects in nanoelectronic devices. Measurements of the ECR of the metallic metal-oxide materials are more difficult because they are mechanically stiffer than ductile metals. Until now, only the stiff material of the carbon nanotube was employed to inspect quantum resistors by using a scanning probe microscope and a soft liquid metal [16, 17]. The liquid metal made a soft contact on the carbon nanotube so the measurement of quantized conductance was feasible.

A combination-type microscope of transmission electron microscope (TEM) and scanning tunneling microscope (STM) (TEM–STM) was developed to begin the visualization of atomic chain deformations [18] and the inspection of the quantized conductance [19] as well as the quantized ECR. In the latest report, stable gold wires with a single-atom width were demonstrated for mechanical and electrical studies [20]. With the help of a progress of nanomaterial syntheses, an TEM–STM was employed for the electrical characterization of individual semiconductor NWs [21, 22], demonstration of bistable nanoelectromechanical devices [23], exploration of contact effects [24–26], studies of electron field emission properties [27], and tailoring of current–voltage behaviors and the electrical contact resistance of metal wires [28]. In our previous study [26], the TEM–STM technique was shown to provide a handy measurement to unveil a nonlinear current–voltage (I–V) curve and a high ECR from the nanocontact. In this work, we utilize the same technique and ECR reducing processes to study both the intrinsic resistivity and the residual ECR of various metallic metal-oxide NWs. A gold tip is used to make one or more relatively soft metal contacts (or taps) on the metal-oxide NWs and the overall ECR from the nanocontacts on the NWs could be evaluated.

2. Experimental details

Metallic metal-oxide NWs of RuO_2, as-implanted and annealed Cu–RuO_2 were employed in TEM–STM measurements. RuO_2 samples were prepared on Si wafer using a standard thermal evaporation method and the preparation methods are described in detail elsewhere [26]. The as-grown RuO_2 NWs were implanted at room temperature with 72 keV Cu ions by using a tandem accelerator (NEC 9SDH-2). The as-implanted Cu–RuO_2 NWs were heated in a high vacuum at 350 °C for 120 h to make annealed NWs. We ascertained that not only the large-scale morphology but also the nanometer roughness on surfaces of the NWs do not alter after prolonged vacuum annealing. The chemical components of the Cu-doped RuO_2 NWs were decided by using energy dispersive x-ray (EDX) spectroscopy. According to EDX spectra, the Cu-doped RuO_2 NWs were determined to be $Ru_{0.98}Cu_{0.02}O_2$ and $Ru_{0.93}Cu_{0.07}O_2$ for Cu ion doses of 1 and 3 $\times$ 10^{16} cm^{-2}, respectively. The morphology, crystalline structures and diameters of all metallic metal-oxide NWs were inspected by using a high-resolution TEM (JEOL JEM-2010F).

Electrical characterizations were obtained in another TEM (JEOL JEM-2000FXII) equipped with a Nanofactory STM on the TEM holder. Electrochemically etched gold wires were used as STM tips. The Si wafer with metallic metal-oxide NWs deposited on it was attached on the STM sample holder by using silver paste to ensure a conducting contact. By using STM, I–V curves were acquired under a high vacuum of 1 $\times$ 10^{-5} Pa at room temperatures when an STM tip was approaching the NW and the TEM electron beam (e-beam) was blanked. The I–V results were taken with voltages ramped from -2 to $+2$ V with a start-up acquisition time of 500 ms and a settling time of 100 ms for every I–V data point. Ten I–V curves were averaged to get a characteristic I–V curve of individual metallic metal-oxide NWs through TEM–STM I–V measurement.

3. Results and discussion

The growth behaviors and the structural characterizations of RuO_2 NWs have been described in previous reports [26]. To check the crystalline structure of pure and Cu-doped RuO_2 NWs, figure 1 presents high-resolution TEM images of pure RuO_2 and as-implanted $Ru_{0.93}Cu_{0.07}O_2$ NWs with electron diffraction patterns in the insets. The TEM images and the electron diffraction patterns support a mostly crystalline structure even after Cu ion implantations. These structural characterizations support the fact that all the metal-oxide NWs used in this study could have comparable electrical properties. A schematic illustration of the TEM–STM electrical measurement is illustrated in figure 1(d).

3.1. ECR reducing processes

Several ECR reducing processes must be adopted for all the metallic metal-oxide NWs under TEM–STM measurements, to extract intrinsic NW resistances. Figure 2(a) presents a typical TEM image of a gold tip contacting on a NW before vacuum annealing. The shadows on the edges of the tip and the NW reveal contamination which could be hydrocarbons reacted with e-beam [29]. The contamination leads to a large tunneling resistance and gives a nonlinear I–V curve in TEM–STM measurements. The hydrocarbon contamination could be prevented by a thermal treatment in which both the STM probe and the NW were heated at 80 °C in a high vacuum for more than 10 h. Subsequently, a mechanical treatment of a pressing and rubbing process is employed to expand the contact area so as to reduce the ECR [30]. The TEM images of a gold tip and a

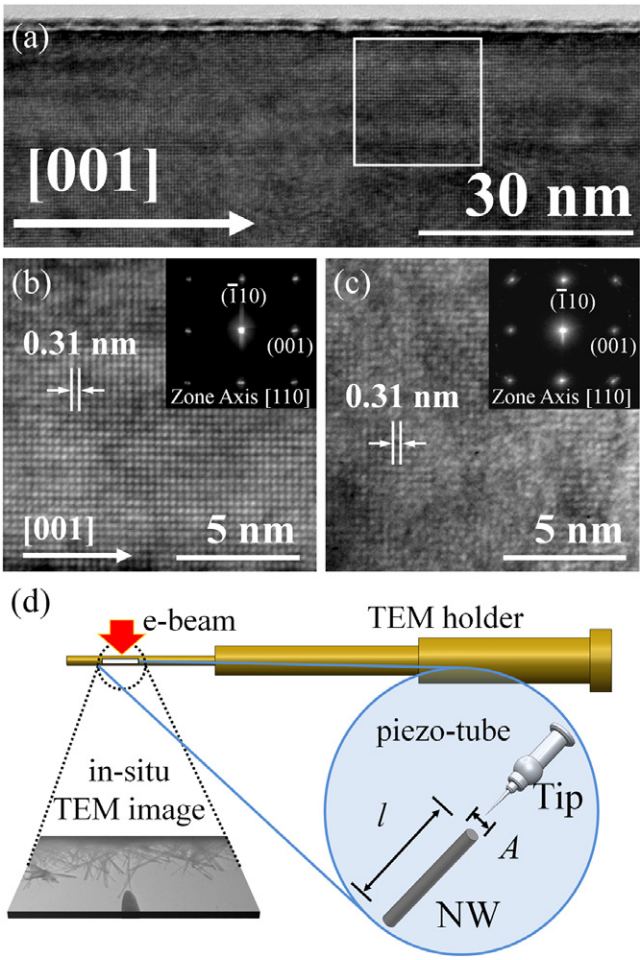

Figure 1. TEM image (a) of a pure RuO_2 NW and a high-resolution TEM image (b) of the white square on (a). (c) High-resolution TEM image of an as-implanted $Ru_{0.93}Cu_{0.07}O_2$ NW. The lattice spacing and the growth direction are indicated on the images. The insets show their corresponding electron diffraction patterns with the zone axis along the [110] direction. (d) Schematic diagram of our experimental setup of an STM on a TEM holder. The image on the bottom illustrates a TEM measurement under the e-beam exposure (red arrow) and the scheme in the right circle points to the dimensions, the length l and area A, of a NW and the configuration of an STM tip approaching the NW.

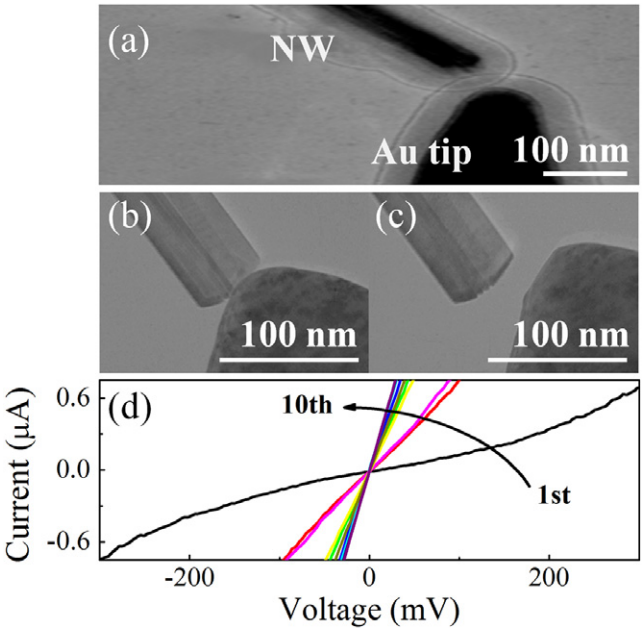

Figure 2. (a) TEM image of an STM tip in contact with a RuO_2 NW before any thermal treatment. TEM images of an STM tip and a RuO_2 NW (b) before and (c) after a pressing and rubbing process. (d) Multiple step (from the first to the tenth step) I–V measurements of a RuO_2 NW before and after thermal, mechanical, and e-beam exposing treatments.

NW before and after the mechanical treatment are displayed in figures 2(b) and (c), respectively. It is worth pointing out that the nanomachining technique can create a flattened area 40 nm in diameter on the gold tip (see figure 2(c)). It corroborates the fact that the metal gold is much more ductile than our metallic metal-oxide NWs. The last ECR reducing process is the e-beam exposing treatment with a dose of 1.5×10^6 C m^{-2} s^{-1} for 10 s when the gold tip is in contact with the NW. After e-beam exposure, we have inspected the TEM images and we have not found any appreciable variations in structure and morphology of the NWs. The I–V curves, before and after going through the three different ECR reducing treatments, are recorded and exposed in figure 2(d). In the continuous monitoring of the I–V behaviors, the current increases by at least two orders of magnitude and the nonlinear I–V curve (the first I–V curve) of the untreated STM tip and NW will be gradually converted to an ohmic line, such as the tenth I–V curve in figure 2(d). The second I–V curve is obtained after vacuum annealing. The third and the fourth I–V curves are measured after pressing and rubbing processes. The tip is maintained to tap on the NW in the following treatments and electrical measurements. The fifth to the tenth I–V curves are taken after each ten-second e-beam exposing step.

3.2. Minimum total resistance

The typical TEM image as shown in figure 3(a) displays the lengths of the two contacts on the NW. The RuO_2 NWs have a rectangular cross section. After the ECR reducing processes, a minimum of a total resistance of each NW can be estimated from the characteristic I–V curve in a low voltage range of ± 10 mV. Total resistances of several tens of NWs of the same system but different dimensions are evaluated. The total resistance R_T exhibits a linear dependence on the ratio of the length (l) to the cross-sectional area (A) of the NWs. Figures 3(b)–(e) demonstrate the experimental data with linear-least-square fittings of the RuO_2, as-implanted $Ru_{0.98}Cu_{0.02}O_2$ and $Ru_{0.93}Cu_{0.07}O_2$, and annealed $Ru_{0.93}Cu_{0.07}O_2$ NWs. The linear dependence of R_T on l/A implies an ohmic behavior, reaching a concordance of an ohmic contact to the linear I–V curve after ECR reducing treatments. Moreover, a temperature dependent resistance measurement, indicating a metal behavior of lower resistances with decreasing temperatures, has been established in two- and four-probe measurements for RuO_2 NWs [26] to support metallic transport in the metal-oxide NWs. Even though we try hard to remove the contact resistance, which comes from the interface between the NW

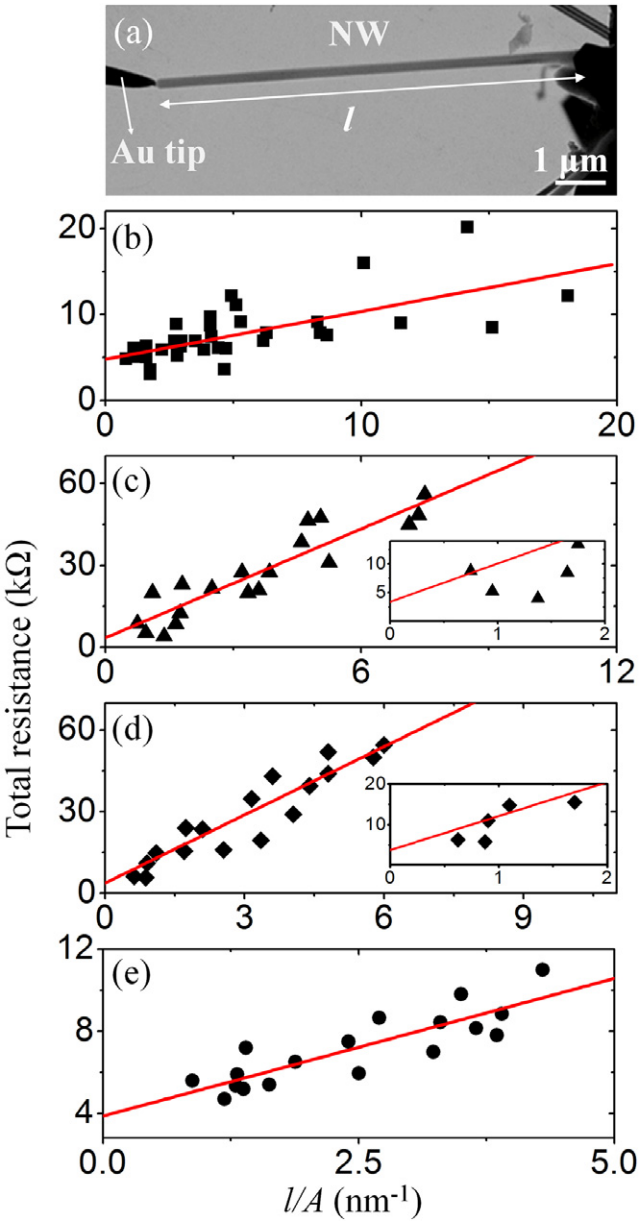

Figure 3. (a) TEM image of a complete RuO_2 NW 5.7 μm in length and 138 nm in width. STM measured resistances as a function of l/A of (b) RuO_2, (c) as-implanted $Ru_{0.98}Cu_{0.02}O_2$, (d) as-implanted $Ru_{0.93}Cu_{0.07}O_2$, and (e) annealed $Ru_{0.93}Cu_{0.07}O_2$ NWs. The solid lines show results of linear least square fittings. The insets show an enlarged scale of the same data near the coordinate origin. The averaged resistivities and residual ECRs are evaluated from the fittings (see text).

and the STM gold tip, we still can see a residual resistance in figure 3 (see the y-axis intercept) for all kinds of metallic metal-oxide NWs. As for the as-implanted Cu–RuO_2 NWs featured in high total resistance, residual resistances are unambiguously identified in the insets of figures 3 (c) and (d) with an enlarged scale.

We notice that the minimum total resistance obtained in our experiments, after the ECR reducing processes, is in the range of one to tens of kilohm. In comparison with TEM–STM electrical measurements of tungsten microwires in a previous report [28], in which a change of resistance from 100 Ω to 1 MΩ is demonstrated due to dynamical alternations of wire-to-electrode-surface angle and the mechanical load exerted on the contacts, our data provide total resistances in a narrow range supporting metallic contacts and free from the contaminants found and concluded in the previous report [28]. The total resistance displayed in figure 3 agrees well with the mathematical form of $R_T = R_C + \rho l/A$, where R_C is the residual ECR. From the above analysis, the average resistivities of RuO_2, as-implanted $Ru_{0.98}Cu_{0.02}O_2$ and $Ru_{0.93}Cu_{0.07}O_2$, and annealed $Ru_{0.93}Cu_{0.07}O_2$ NWs are estimated to be 55 ± 10, 644 ± 90, 836 ± 103, and 146 ± 39 $\mu\Omega$ cm, respectively. In addition, the average resistivity, ~55 $\mu\Omega$ cm, of the RuO_2 NW approaches a near bulk resistivity of ~35 $\mu\Omega$ cm at room temperature [31, 26]. The agreements backs up again our measurements of average resistivities of the metallic metal-oxide NWs. On the other hand, the fitting in figure 3 brings about the residual ECRs of 5 ± 0.7, 3.4 ± 1.9, 3.7 ± 2.1, and 3.7 ± 1.1 kΩ for RuO_2, as-implanted $Ru_{0.98}Cu_{0.02}O_2$ and $Ru_{0.93}Cu_{0.07}O_2$, and annealed $Ru_{0.93}Cu_{0.07}O_2$ NWs, respectively.

3.3. Electrical contact resistance (ECR)

It is noticed that the averaged residual ECR ranged from 3.4 to 5 kΩ while the average resistivities ranged from 55 to 836 $\mu\Omega$ cm for our metallic metal-oxide NWs. In contrast to a change of one order of magnitude in average resistivities, the small variation in residual ECR drives us to examine the nature of electrical properties in the interfacial contact between the gold tip and the NW. In the beginning, we conjecture that the ECR results from a gold nanoneck or nanocontact. Since gold is a highly ductile material, a gold nanocontact can form not only wires with single-atom width [20] but also a thick neck with a cross-sectional diameter of several tens of nanometers [9]. The ECR reducing process of the mechanical treatment in which the tip is pressed against the NW could assist in building a thick gold neck and result in a very low ECR, less than 100 Ω. The ECR built up from a pure gold nanocontact is too small to explain our experimental result and the gold atom is too big to diffuse into the metallic metal-oxide NW so we can exclude this possibility.

We change over to conjecture that the kilohm ECR originates from the nanocontact on the metallic metal-oxide NW. In a similar way to using liquid metal to make a soft contact on a stiff carbon nanotube [16, 17], the gold, in comparison with the NW (see figures 2(b) and (c)), is ductile to make one or more taps on the metallic metal-oxide NW. We are, therefore, able to detect a constriction resistance from the NW. The nanometer roughness on RuO_2 and Cu-doped RuO_2 NWs is perceptible in figures 4(a)–(c). The small roughness could be regarded as protrusions with a cross-sectional diameter of ~3 nm on the surfaces of the NWs. Under the ECR reducing process of the mechanical treatment, the gold tip could be nanomachined to form a flattened surface (figure 2(c)) and to make at least one tap on the surface protrusions of the metal-oxide NWs. A schematic diagram of the gold contact on the NW is given in figure 4(d).

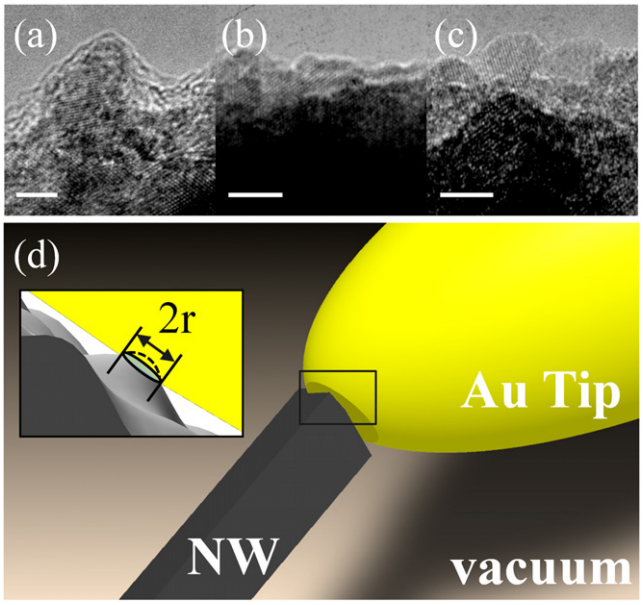

Figure 4. TEM images of nanometer roughness on (a) RuO_2, (b) as-implanted $Ru_{0.98}Cu_{0.02}O_2$, and (c) as-implanted $Ru_{0.93}Cu_{0.07}O_2$ NWs with a scale bar of 3 nm in length. (d) A schematic diagram to model the flattened surface of a gold tip in contact with the nanometer rough surface of a metallic metal-oxide NW. The inset shows a close view of the rectangle area (the nanocontact).

The effective mass and the Fermi velocity of electrons in RuO_2 bulk are 1.4 m_e and 0.28 $\times$ 10^6 m s^{-1} [32, 33] to give a Fermi wavelength (λ_F) of about 2 nm. If we consider one tap, using the cross-sectional area of the protrusion as the nanocontact on the NW, we can apply the semiclassical Sharvin approximation of $(\lambda_F/\pi r)^2(h/2e^2)$ to the calculation of the constriction resistance. The calculated ECR is $\sim$2 kΩ, which is in line with our experimental data, for a nanocontact with a radius $r = 1.5$ nm. More elaborate calculations, considering the atomic orbital, the arrangements of atomic chains, and the interface between the NW and the gold tip, are left for further studies. Series connected nanodevices through these metallic metal-oxide nanocontacts could result in a high resistance so we come to the conclusion that metallic metal-oxide nanocontacts 3 nm in diameter are not suitable for applications as interconnects in some low-resistance nanoelectronic devices.

3.4. Structural ordering induced resistivity variation

In addition to the study of nanocontact ECR, the TEM–STM can be adopted to measure the average resistivity of NWs. The variation in electrical properties with a modulation of the structural ordering and the doping could be learned as well. In our previous discussions, we have unearthed that the average resistivities of RuO_2, as-implanted $Ru_{0.98}Cu_{0.02}O_2$ and $Ru_{0.93}Cu_{0.07}O_2$, and annealed $Ru_{0.93}Cu_{0.07}O_2$ NWs are about 55, 644, 836, and 146 $\mu\Omega$ cm. The average resistivity rises by more than one order of magnitude after Cu ion implantations and it drops to a much smaller value after high-vacuum annealing. The outcome implies the destruction of crystalline structures by Cu ion bombardments. It is noted that the variation of crystalline structures in bulk can be observed by x-ray diffraction. The NWs are prepared by ion implantation after the growth of a 3 μm thick layer of clustered RuO_2 NWs and only a thin layer near the top about a hundred nanometers thick is clustered Cu-doped RuO_2 NWs. The penetration depth of the x-ray diffraction measurement is much longer than the thickness of the clustered Cu-doped RuO_2 NWs so we turn to observe structural order in electron diffraction patterns and Fourier transformed images. The technique was adopted in a previous paper of Co-doped ZnO NWs as well [34]. Although the technique is spatially limited and indicative due to its probe of minimum volumes of individual NWs, we provide more data for each NW system and statistical analysis to corroborate the following statements. We return to examine the NW crystalline structure in high-resolution TEM images displayed in figure 5. The lattice lines extend to cover the whole image on figures 5(a) and (d), suggesting that the as-grown RuO_2 and annealed $Ru_{0.93}Cu_{0.07}O_2$ NWs have a high crystalline ordering in contrast to the as-implanted Cu–RuO_2 NWs. In order to drag structural ordering out of the high-resolution TEM images, the corresponding fast-Fourier-transformed images are calculated and exhibited in the insets of figure 5. For the as-implanted Cu–RuO_2 NWs, the reciprocal lattice points blur to form disks or halos in the insets of figures 5(b) and (c).

Indicative results of structural orderings are given in figure 6. A line spectrum from the center to the satellite points on the fast-Fourier-transformed image is introduced in figure 6(a) to unveil the intensity distribution of the peak of the reciprocal lattice point. A linewidth (full width at half maximum) of the peak, which is related to the broadening of the reciprocal lattice point as well as the disordering of lattice structure, can be estimated. Figure 6(b) describes the result of linewidths with regard to the Cu concentration and the heat treatment. The results obtained from Fourier transformed images are consistent with those obtained from electron diffraction patterns (not shown). We have an indication of structural ordering from the linewidth for the as-implanted and annealed $Ru_{0.93}Cu_{0.07}O_2$ NWs to corroborate our suggestion of structure destruction from ion bombardments. On the other hand, the linewidth for the as-implanted and annealed $Ru_{0.98}Cu_{0.02}O_2$ NWs does not make appreciable changes. In fact, the average resistivity of the annealed $Ru_{0.98}Cu_{0.02}O_2$ NWs (not shown in figure 3) is about 40 $\mu\Omega$ cm which is smaller than one tenth of that of the as-implanted NWs. From the result, we draw the conclusion that other structural defects, which are cannot be inspected in TEM images, might give rise to a high average resistivity of the as-implanted NWs. Moreover, to compare the average resistivities of RuO_2 NWs with those of the annealed $Ru_{0.93}Cu_{0.07}O_2$ and $Ru_{0.98}Cu_{0.02}O_2$ NWs, we have discovered that the room-temperature resistivity of RuO_2 NWs increases after the introduction of Cu ions.

4. Conclusions

In summary, RuO_2 NWs have been synthesized by thermal evaporation and Cu-doped RuO_2 NWs are made by ion implantations. The as-implanted Cu–RuO_2 NWs are thermally treated in a high vacuum to give annealed NWs. All the metal-oxide NWs are examined in high-resolution TEM to ensure

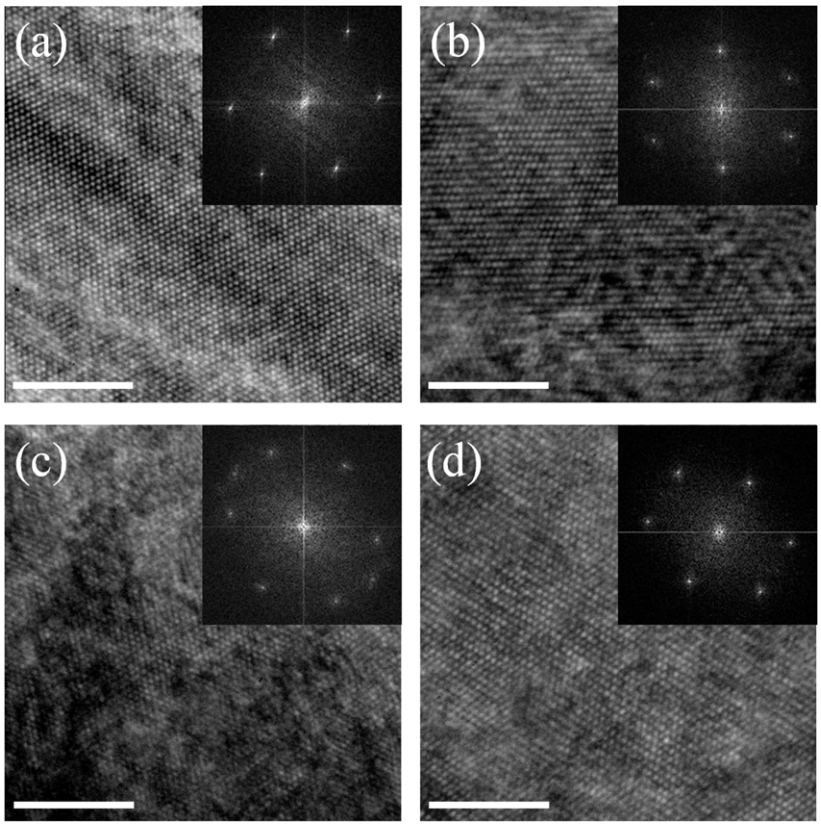

Figure 5. High-resolution TEM images with corresponding fast-Fourier-transformed patterns of (a) RuO_2, (b) $Ru_{0.98}Cu_{0.02}O_2$, (c) $Ru_{0.93}Cu_{0.07}O_2$, and (d) annealed $Ru_{0.93}Cu_{0.07}O_2$ NWs. A scale bar of 5 nm in length is marked in the figures.

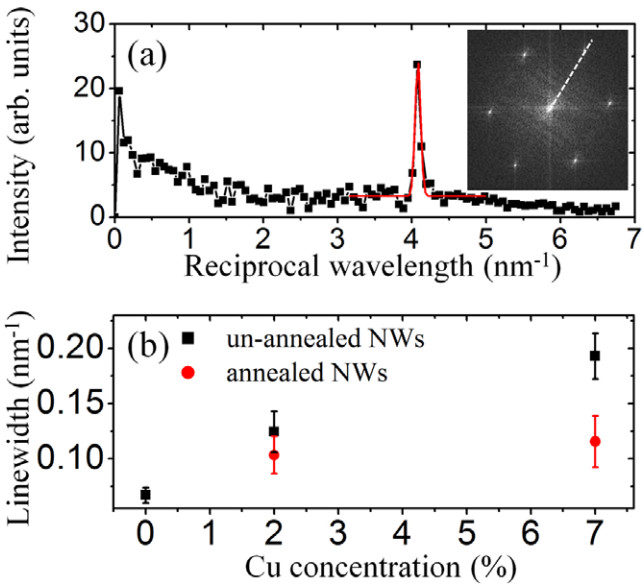

Figure 6. (a) Radial intensity of the line drawn on the two-dimensional fast-Fourier-transformed image (inset) of a RuO_2 NW. The red curve points out the peak distribution of a reciprocal lattice point for the linewidth estimation. (b) The linewidth of reciprocal lattice points of the as-implanted (un-annealed) and annealed Cu–RuO_2 NWs with different Cu concentration.

a mostly crystalline structure and a comparable electrical property. The NWs are applied to TEM–STM measurements to obtain I–V curves and zero-voltage resistance. ECR reducing processes, including vacuum annealing, mechanical pressing and rubbing, and e-beam exposing treatments, are employed to reduce the contact resistance and to acquire minimum total resistances of individual NWs. However, the contact resistance cannot be totally removed. Resistances of several tens of the same kind of metal-oxide NWs are acquired to demonstrate the linear dependence on the ratio of the length to the area of the NWs to estimate the average resistivity and the residual ECR.

The residual ECRs of all metallic metal-oxide NWs are in the small range from 3.4 to 5 kΩ while the average resistivities change by more than one order of magnitude. We argued that the kilohm ECR could originate from the constriction resistance of the NW nanocontacts on which the gold tip can make one or more taps on the NWs for electrical characterizations. TEM images and a simple calculation support our conjecture. On the other hand, the change of average resistivities of the as-implanted and the annealed Cu–RuO_2 NWs reveals destruction on crystalline structures after ion bombardments that can be estimated in the linewidth of the reciprocal lattice points on the Fourier transformed images. A higher room-temperature resistivity due to an introduction of Cu ions in the RuO_2 NWs has been discovered as well.

Acknowledgments

This work was supported by the Taiwan National Science Council under grant No. NSC 95-2112-M-009-045-MY3 and by the MOE ATU Program.

References

[1] Greenwood J A 1966 *Br. J. Appl. Phys.* **17** 1621
[2] Kogut L and Komvopoulos K 2003 *J. Appl. Phys.* **94** 3153
[3] Agraït N, Yeyati A L and van Ruitenbeek J M 2003 *Phys. Rep.* **377** 81
[4] Landauer R 1957 *IBM J. Res. Dev.* **1** 223
[5] Wharam D A, Thornton T J, Newbury R, Pepper M, Ahmed H, Frost J E F, Hasko D G, Peacock D C, Ritchie D A and Jones G A C 1988 *J. Phys. C: Solid State Phys.* **21** L209
[6] van Wees B J, van Houten H, Beenakker C W J, Williamson J G, Kouwenhoven L P, van der Marel D and Foxon C T 1988 *Phys. Rev. Lett.* **60** 848
[7] Muller C J, van Ruitenbeek J M and de Jongh L J 1992 *Phys. Rev. Lett.* **69** 140
[8] Agraït N, Rodrigo J G and Vieira S 1993 *Phys. Rev.* B **47** 12345
[9] Jian W B, Chang C S, Li W Y and Tsong T T 1999 *Phys. Rev.* B **59** 3168
[10] Hansen K, Lægsgaard E, Stensgaard I and Besenbacher F 1997 *Phys. Rev.* B **56** 2208
[11] Terabe K, Hasegawa T, Nakayama T and Aono M 2005 *Nature* **433** 47
[12] Costa-Krämer J L, García P, García-Mochales N and Serena P A 1995 *Surf. Sci.* **342** L1144
[13] Ittah N, Yutsis I and Selzer Y 2008 *Nano Lett.* **8** 3922
[14] Pauly F, Dreher M, Viljas J K, Häfner M, Cuevas J C and Nielaba P 2006 *Phys. Rev.* B **74** 235106
[15] Vadimsky R G, Frankenthal R P and Thompson D E 1979 *J. Electrochem. Soc.* **126** 2017
[16] Frank S, Poncharal P, Wang Z L and de Heer W A 1998 *Science* **280** 1744
[17] Poncharal P, Berger C, Yi Y, Wang Z L and de Heer W A 2002 *J. Phys. Chem.* B **106** 12104
[18] Kizuka T 1998 *Phys. Rev.* B **57** 11158
[19] Ohnishi H, Kondo Y and Takayanagi K 1998 *Nature* **395** 780
[20] Kizuka T 2008 *Phys. Rev.* B **77** 155401
[21] Larsson M W, Wallenberg L R, Persson A I and Samuelson L 2004 *Microsc. Microanal.* **10** 41
[22] Zhang Z Y, Jin C H, Liang X L, Chen Q and Peng L M 2006 *Appl. Phys. Lett.* **88** 073102
[23] Ziegler K J, Lyons D M, Holmes J D, Erts D, Polyakov B, Olin H, Svensson K and Olsson E 2004 *Appl. Phys. Lett.* **84** 4074
[24] Zhang Z, Yao K, Liu Y, Jin C, Liang X, Chen Q and Peng L M 2007 *Adv. Funct. Mater.* **17** 2478
[25] Takeguchi M, Shimojo M, Tanaka M, Che R, Zhang W and Furuya K 2006 *Surf. Interface Anal.* **38** 1628
[26] Liu Y L, Wu Z Y, Lin K J, Huang J J, Chen F R, Kai J J, Lin Y H, Jian W B and Lin J J 2007 *Appl. Phys. Lett.* **90** 013105
[27] Jin C H, Zhang Z Y, Wang J Y, Chen Q and Peng L M 2006 *Appl. Phys. Lett.* **89** 213108
[28] Costa P M F J, Fang X, Wang S, He Y, Bando Y, Mitome M, Zou J, Huang H and Golberg D 2009 *Microsc. Res. Tech.* **72** 93
[29] Wang Y G, Wang T H, Lin X W and Dravid V P 2006 *Nanotechnology* **17** 6011
[30] Lin Y F and Jian W B 2008 *Nano Lett.* **8** 3146
[31] Ryden W D, Lawson A W and Sartian C C 1970 *Phys. Rev.* B **1** 1494
[32] Glassford K M and Chelikowsky J R 1994 *Phys. Rev.* B **47** 1732
[33] Glassford K M and Chelikowsky J R 1994 *Phys. Rev.* B **49** 7107
[34] Wu Z Y, Chen F R, Kai J J, Jian W B and Lin J J 2006 *Nanotechnology* **17** 5511